Collective Excitations of Quantum Anomalous Hall Ferromagnets in Twisted Bilayer Graphene

Fengcheng Wu and Sankar Das Sarma
Condensed Matter Theory Center and Joint Quantum Institute, Department of Physics, University of Maryland, College Park, Maryland 20742, USA

(Received 20 August 2019; published 30 January 2020)

We present a microscopic theory for collective excitations of quantum anomalous Hall ferromagnets (QAHF) in twisted bilayer graphene. We calculate the spin magnon and valley magnon spectra by solving Bethe-Salpeter equations and verify the stability of QAHF. We extract the spin stiffness from the gapless spin wave dispersion and estimate the energy cost of a skyrmion-antiskyrmion pair, which is found to be comparable in energy with the Hartree-Fock gap. The valley wave mode is gapped, implying that the valley polarized state is more favorable compared to the valley coherent state. Using a nonlinear sigma model, we estimate the valley ordering temperature, which is considerably reduced from the mean-field transition temperature due to thermal excitations of valley waves.

DOI: 10.1103/PhysRevLett.124.046403

Introduction.—Twisted bilayer graphene (TBG) near the magic angle hosts a plethora of phenomena, e.g., superconductivity [1], correlated insulators [2], nematicity [3,4], large linear-in-temperature resistivity [5,6], quantum anomalous Hall effect (QAHE) [7,8], etc. Because of this richness, TBG and related moiré systems are currently under intense experimental [1–18] and theoretical [19–62] study. For QAHE, which is the focus of this Letter, moiré bilayers emerge as a new and clean system [8,9] to realize Chern insulators at elevated temperatures compared with the magnetic topological insulators [63].

Moiré superlattices in van der Waals bilayers not only generate nearly flat bands but also often endow the bands with nontrivial topology. In moiré systems with valley contrast Chern numbers, the enhanced electron Coulomb repulsion effect due to band flattening can spontaneously break the valley degeneracy, and therefore, lead to valley polarized states with QAHE [49–55]; we term such bulk insulating states as quantum anomalous Hall ferromagnets (QAHFs), in analogy with the well-known quantum Hall ferromagnets (QHFs) [64,65]. In pristine TBG, $\hat{C}_{2z}$ symmetry (a twofold rotation around the out-of-plane axis) combined with time-reversal symmetry forbids Berry curvature. However, this $\hat{C}_{2z}$ symmetry can be explicitly broken when TBG is aligned to the hexagonal boron nitride (hBN) substrate, generating a nonzero valley Chern number. It is in this extrinsic TBG aligned with hBN where the anomalous Hall effect [7] and later its quantized version (QAHE) [8] have been observed at the filling factor $\nu = 3$. Here we define ν as n/n_0, where n is the electron density and n_0 the density for one electron per moiré unit cell.

In this Letter, we theoretically study the collective excitations in the TBG QAHF in order to examine the QAHF stability and to determine the low-energy excitations that control the transport gap and that limit the ferromagnetic transition temperature. The $\nu = 3$ QAHF in extrinsic TBG has two distinct collective excitations, i.e., spin magnons and valley magnons, which involve particle-hole transitions with, respectively, a single spin flip and a single valley flip. We calculate the energy spectra separately for the two types of magnons by solving their Bethe-Salpeter equations. The calculated excitation spectra indicate that the TBG QAHF is generally robust against small particle-hole fluctuations when the bulk Hartree-Fock gap (Δ_{HF}) is finite. The spin magnon spectrum has a gapless spin wave mode, which is the Goldstone mode due to the spontaneous breaking of the spin SU(2) symmetry in the $\nu = 3$ QAHF. We extract spin stiffness from the long-wavelength spin wave dispersion and estimate the skyrmion energy. We find that the energy Δ_{pair} for a pair of skyrmion and antiskyrmion in the TBG QAHF is comparable in energy with Δ_{HF}, and either Δ_{pair} or Δ_{HF} can be the lowest charged excitation gap depending on the details of the system.

In a two-dimensional system such as TBG with spin SU(2) symmetry, the spin ordering temperature vanishes according to the Mermin-Wagner theorem. However, QAHE in TBG can arise purely from an orbital effect, e.g., valley polarization. An important distinction between spin and valley is that there is only a valley U(1) symmetry in TBG in contrast to the spin SU(2) symmetry. The $\nu = 3$ QAHF preserves the valley U(1) symmetry but breaks the discrete time-reversal symmetry, which allows a finite valley ordering temperature T_V. We estimate T_V based on the fully gapped valley magnon spectrum and find that T_V is reduced from the mean-field transition temperature due to thermal excitations of valley waves, which provides

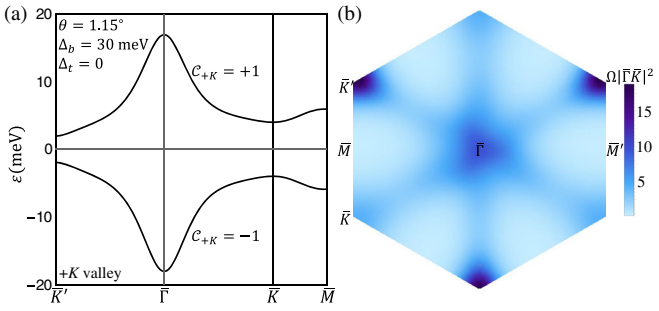

FIG. 1. (a) The $+K$-valley moiré band structure with $\theta = 1.15°$ and $(\Delta_b, \Delta_t) = (30, 0)$ meV. (b) Berry curvature Ω of the first moiré conduction band in (a). We use a definition of Ω such that an occupied band with a Chern number $\mathcal{C}$ contributes $+\mathcal{C}e^2/h$ to the Hall conductivity σ_{xy}.

an explanation for the experimentally observed hierarchy that the transport energy gap of the TBG QAHF is larger than the corresponding Curie temperature [8].

Ferromagnetism.—We calculate the moiré band structure of TBG using the continuum Hamiltonian [66], with details given in the Supplemental Material [67]. We use parameter Δ_b (Δ_t) to describe the sublattice potential difference in the bottom (top) graphene layer and take $(\Delta_b, \Delta_t) = (30, 0)$ meV [68] in order to simulate the experimental situation [7,8] where TBG is in close alignment to one of the two (either top or bottom) encapsulating hBN layers. The corresponding moiré band structure in the $+K$ valley at twist angle $\theta = 1.15°$ is shown in Fig. 1, where the first moiré conduction and valence bands are separated by an energy gap about 4 meV (opened up by Δ_b) and, respectively, carry a Chern number $\mathcal{C}$ of $+1$ and -1. Because of time-reversal symmetry, the first moiré conduction (valence) band in the $-K$ valley has a $\mathcal{C}$ value of -1 ($+1$).

We study a minimal interacting model by retaining only the first moiré conduction band states, assuming that all valence band states are filled. The projected Hamiltonian H has the single-particle term H_0 and the interacting term H_1,

$$\begin{aligned} H_0 &= \sum_{\boldsymbol{k},\tau,s} \varepsilon_{\boldsymbol{k},\tau} c^\dagger_{\boldsymbol{k},\tau,s} c_{\boldsymbol{k},\tau,s}, \\ H_1 &= \frac{1}{2A} \sum V^{(\tau\tau')}_{\boldsymbol{k}_1\boldsymbol{k}_2\boldsymbol{k}_3\boldsymbol{k}_4} c^\dagger_{\boldsymbol{k}_1,\tau,s} c^\dagger_{\boldsymbol{k}_2,\tau',s'} c_{\boldsymbol{k}_3,\tau',s'} c_{\boldsymbol{k}_4,\tau,s}, \\ V^{(\tau\tau')}_{\boldsymbol{k}_1\boldsymbol{k}_2\boldsymbol{k}_3\boldsymbol{k}_4} &= \sum_{\boldsymbol{q}} V(\boldsymbol{q}) O^{(\tau)}_{\boldsymbol{k}_1\boldsymbol{k}_4}(\boldsymbol{q}) O^{(\tau')}_{\boldsymbol{k}_2\boldsymbol{k}_3}(-\boldsymbol{q}), \\ O^{(\tau)}_{\boldsymbol{k}\boldsymbol{k}'}(\boldsymbol{q}) &= \int d\boldsymbol{r} e^{i\boldsymbol{q}\cdot\boldsymbol{r}} \Phi^*_{\boldsymbol{k},\tau}(\boldsymbol{r}) \Phi_{\boldsymbol{k}',\tau}(\boldsymbol{r}), \end{aligned} \tag{1}$$

where $c^\dagger_{\boldsymbol{k},\tau,s}$, $\varepsilon_{\boldsymbol{k},\tau}$, and $\Phi_{\boldsymbol{k},\tau}$ are, respectively, the fermion creation operation, moiré band energy, and wave function of the first conduction band state with spin label s, valley index τ, and momentum $\boldsymbol{k}$. Because of the time-reversal symmetry, $\varepsilon_{\boldsymbol{k},\tau} = \varepsilon_{-\boldsymbol{k},-\tau}$ and $\Phi_{\boldsymbol{k},\tau} = \Phi^*_{-\boldsymbol{k},-\tau}$, where $\boldsymbol{k}$ is measured relative to the moiré Brillouin zone center $\bar{\Gamma}$ point. In H_1, A is the system area, $O^{(\tau)}_{\boldsymbol{k}\boldsymbol{k}'}(\boldsymbol{q})$ is the density matrix element, and $V(\boldsymbol{q})$ is the screened Coulomb potential $2\pi e^2 \tanh(qd)/(\epsilon q)$, where ϵ is the effective dielectric constant, and d is the vertical distance between TBG and the top (bottom) metallic gates. We take d to be 40 nm as in the experiment of Ref. [8] and ϵ as a free parameter since screening in TBG can be quite complicated. The dielectric screening from the encapsulating hBN should set a lower bound on ϵ, leading to $\epsilon > 5$ in our model. ϵ also effectively controls the ratio between interaction and bandwidth. In TBG, the bandwidth near the magic angle is not exactly known experimentally, which is another good reason to take ϵ as a free parameter.

Hamiltonian H has spin SU(2) and valley U(1) symmetry. We use the Hartree-Fock (HF) approximation and assume that the valley U(1) symmetry is preserved but allow spin and valley polarization, which leads to the following mean-field Hamiltonian

$$\begin{aligned} H_{\mathrm{MF}} &= \sum_{\boldsymbol{k},\tau,s} E_{\boldsymbol{k},\tau,s} c^\dagger_{\boldsymbol{k},\tau,s} c_{\boldsymbol{k},\tau,s}, \\ E_{\boldsymbol{k},\tau,s} &= \varepsilon_{\boldsymbol{k},\tau} + \frac{1}{A} \sum_{\boldsymbol{k}',\tau',s'} V^{(\tau\tau')}_{\boldsymbol{k}\boldsymbol{k}'\boldsymbol{k}'\boldsymbol{k}} n_F(E_{\boldsymbol{k}',\tau',s'}) \\ &\quad - \frac{1}{A} \sum_{\boldsymbol{k}'} V^{(\tau\tau)}_{\boldsymbol{k}\boldsymbol{k}'\boldsymbol{k}\boldsymbol{k}'} n_F(E_{\boldsymbol{k}',\tau,s}), \end{aligned} \tag{2}$$

where the quasiparticle energy $E_{\boldsymbol{k},\tau,s}$ includes moiré band energy and Hartree as well as Fock self-energies, and n_F is the Fermi-Dirac occupation number.

We focus on integer filling factors $\nu = 1$, 2, and 3, and make a zero-temperature ($T = 0$) ground state ansatz so that ν out of the 4 first moiré conduction bands (including spin and valley degeneracies) is filled, while the remaining $4 - \nu$ bands are empty. At $\nu = 1$ and 3, the ansatz leads to maximally spin and valley polarized states, which are QAHF and also exact eigenstates of the Hamiltonian H. At $\nu = 2$, this ansatz generates two distinct types of states, namely, a valley polarized state with QAHE and a valley unpolarized state without QAHE, which are energetically degenerate at this particular filling, but it is conceivable that a short-range atomic scale interaction (not included in our Hamiltonian H) may break this degeneracy. We calculate the $T = 0$ HF energy gap Δ_{HF} between empty and occupied bands, as shown in Fig. 2(a). A positive Δ_{HF} indicates the above ansatz is a good candidate for ground states at least in the HF approximation. As expected, Δ_{HF} decreases with increasing dielectric constant ϵ because of the decreasing interaction strength. Δ_{HF} has a strong filling factor dependence, mainly because the Hartree self-energy varies strongly with the electron density [29]. The gap Δ_{HF} at $\nu = 3$ is smaller compared to those at $\nu = 1$ and 2 for small ϵ, but this order is reversed for large ϵ. By fitting to the experimental $\nu = 3$ gap

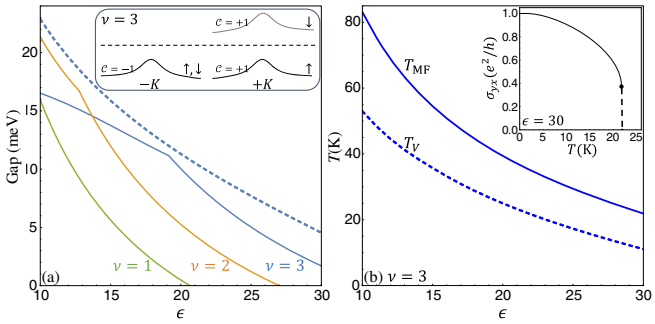

FIG. 2. (a) Charged excitation gap as a function of dielectric constant ϵ. The solid lines are the HF gap Δ_{HF}, respectively, for the three integer filling factors. The dashed line is the skyrmion-antiskyrmion pair energy Δ_{pair} at $\nu = 3$. The inset schematically illustrates the QAHF at $\nu = 3$. (b) Transition temperature at $\nu = 3$ as a function of ϵ. The solid line shows the mean-field transition temperature T_{MF}, and the dashed line shows the valley ordering temperature T_V estimated using the valley wave spectrum. The inset presents the mean-field value of the anomalous Hall conductivity σ_{yx}, where the dashed line marks a jump in σ_{yx} at T_{MF}. All calculations with interaction effects are done on a $36 \times 36\,k$ mesh.

($\sim$2 meV) reported in Ref. [8], we estimate ϵ to be about 30 in our model. With this value of ϵ, we find that the $\nu = 1$ and 2 states are not fully gapped in contrast to $\nu = 3$, which is consistent with experimental findings in Ref. [8]. Therefore, our minimal model does capture the essential experimental phenomenology [8] provided ϵ is tuned to simulate screening of Coulomb interaction, most likely by all the other moiré bands neglected in our theory.

We show the calculated mean-field ferromagnetic transition temperature T_{MF} at $\nu = 3$ in Fig. 2(b). $T_{\mathrm{MF}}(\epsilon = 30)$ is about 22 K, which is larger than the experimental Curie temperature ($\sim$9 K) [8]. We argue that this discrepancy is due to valley wave excitations, which limit the valley ordering temperature, as will be discussed in the following. The anomalous Hall conductivity σ_{yx} at $\nu = 3$ is quantized to e^2/h within 0.3% accuracy up to $T = 3$ K as shown in Fig. 2(b). We numerically find that T_{MF} marks a first-order transition between phases with and without spin-valley polarization, which leads to a jump in σ_{yx} at T_{MF} [Fig. 2(b)]. Remarkably, the experimental anomalous Hall resistance R_{xy} in Ref. [8] also displays a sizable jump near the Curie temperature.

Spin wave.—We examine the stability of the QAHF by studying the collective excitation spectrum. The spin magnon state at $\nu = 3$ can be parametrized as follows:

$$|\boldsymbol{Q}\rangle_S = \sum_{\boldsymbol{k}} z_{\boldsymbol{k},\boldsymbol{Q}} c^{\dagger}_{\boldsymbol{k}+\boldsymbol{Q},+,\downarrow} c_{\boldsymbol{k},+,\uparrow} |\nu = 3\rangle, \tag{3}$$

where $|\nu = 3\rangle$ is the QAHF state in which only the valley $+K$ and spin $\downarrow$ band is empty, $z_{\boldsymbol{k},\boldsymbol{Q}}$ are variational parameters, and $\boldsymbol{Q}$ defined within the first moiré Brillouin zone is the momentum of the magnon. In the magnon state $|\boldsymbol{Q}\rangle_S$, we make a single spin flip from the occupied spin $\uparrow$ band to unoccupied spin $\downarrow$ band within the same $+K$ valley. Variation of the magnon energy with respect to $z_{\boldsymbol{k},\boldsymbol{Q}}$ leads to the following eigenvalue problem:

$$\mathcal{E}_S(\boldsymbol{Q}) z_{\boldsymbol{k},\boldsymbol{Q}} = \sum_{\boldsymbol{k}'} \mathcal{H}^{(\boldsymbol{Q})}_{\boldsymbol{k}\boldsymbol{k}'} z_{\boldsymbol{k}',\boldsymbol{Q}},$$
$$\mathcal{H}^{(\boldsymbol{Q})}_{\boldsymbol{k}\boldsymbol{k}'} = (E_{\boldsymbol{k}+\boldsymbol{Q},+,\downarrow} - E_{\boldsymbol{k},+,\uparrow})\delta_{\boldsymbol{k},\boldsymbol{k}'} - \frac{1}{A} V^{(++)}_{\boldsymbol{k}'(\boldsymbol{k}+\boldsymbol{Q})(\boldsymbol{k}'+\boldsymbol{Q})\boldsymbol{k}}, \tag{4}$$

where the first part in $\mathcal{H}^{(\boldsymbol{Q})}_{\boldsymbol{k}\boldsymbol{k}'}$ is the quasiparticle energy cost of the particle-hole transition, and the second part represents the electron-hole attraction. Equation (4) is typically called the Bethe-Salpeter equation representing repeated electron-hole interactions ("ladder diagrams"), in the context of excitons in semiconductors; here it gives rise to the spin wave spectrum. We note that $\mathcal{H}^{(\boldsymbol{Q})}_{\boldsymbol{k}\boldsymbol{k}'}$ is not gauge invariant (except at $\boldsymbol{Q} = 0$) due to the phase ambiguity of the wave function. However, only closed loops in the momentum space appear in the characteristic polynomial of $\mathcal{H}^{(\boldsymbol{Q})}_{\boldsymbol{k}\boldsymbol{k}'}$, making its eigenvalues gauge invariant; products of wave function overlap along the closed loops encode information of Berry curvature and quantum geometry [69].

We numerically solve Eq. (4) and show the spin excitation spectrum in Fig. 3. The lowest energy mode (spin wave) is gapless at $\boldsymbol{Q} = 0$, which is expected from Goldstone's theorem, as the continuous spin SU(2) symmetry is spontaneously broken in the QAHF. Because of the spin SU(2) symmetry, the spin lowering operator $\sum_{\boldsymbol{k}} c^{\dagger}_{\boldsymbol{k},\tau,\downarrow} c_{\boldsymbol{k},\tau,\uparrow}$ commutes with the Hamiltonian H. Therefore, $z_{\boldsymbol{k},\boldsymbol{Q}} = 1$ for any $\boldsymbol{k}$ is an exact zero-energy solution to Eq. (4) at $\boldsymbol{Q} = 0$. The overall spin excitation spectrum is nonnegative in the parameter space that we have explored (ϵ up to 30), showing the stability of the QAHF at $\nu = 3$ against spin wave excitations.

The spin wave mode can be phenomenologically described using an $O(3)$ nonlinear sigma model [70]

$$\mathcal{L}_S = -\int d^2\boldsymbol{r} \left\{ \frac{\hbar n_0}{2} \boldsymbol{\mathcal{A}}[\boldsymbol{m}] \cdot \partial_t \boldsymbol{m} + \frac{\rho_s}{2} (\boldsymbol{\nabla m})^2 \right\}, \tag{5}$$

where the unit vector $\boldsymbol{m}$ represents the local spin polarization, $\mathcal{A}[\boldsymbol{m}]$ is the effective spin gauge field defined by $\boldsymbol{\nabla}_{\boldsymbol{m}} \times \mathcal{A}[\boldsymbol{m}] = \boldsymbol{m}$, and ρ_s the spin stiffness. We estimate ρ_s by fitting the numerical spin wave spectrum around $\boldsymbol{Q} = 0$ shown in Fig. 3 to the analytical spin wave dispersion $\mathcal{E}_{\mathrm{SW}} = (2\rho_s/n_0)\boldsymbol{Q}^2$ given by Eq. (5). In addition to spin waves, the Lagrangian $\mathcal{L}_S$ also supports skyrmion excitations, which are expected to be charged in the case of QAHF, similar to the QHF case [64]. A pair of skyrmion and antiskyrmion has a total energy cost of $\Delta_{\mathrm{pair}} = 8\pi\rho_s$. We calculate Δ_{pair} using ρ_s estimated above, and find that

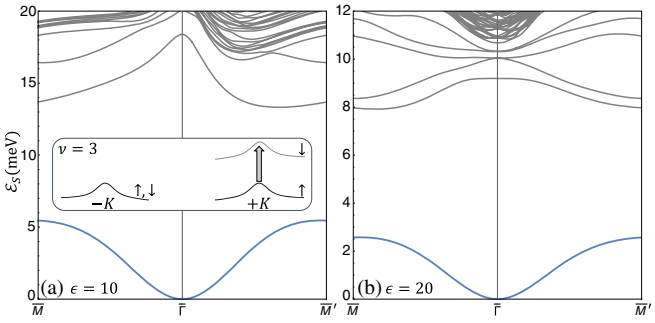

FIG. 3. Excitation spectrum for $\nu = 3$ spin magnon states [inset in (a) for illustration]. The blue lines in (a) and (b) represent the gapless spin wave mode.

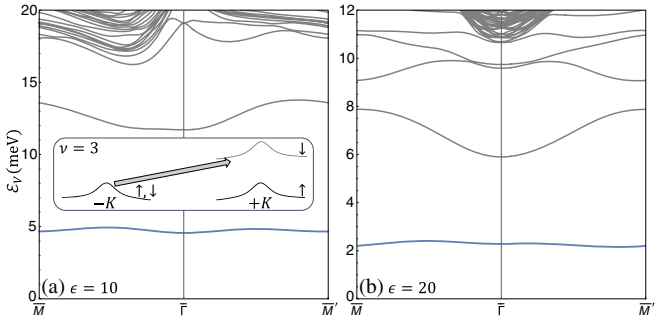

FIG. 4. Excitation spectrum for $\nu = 3$ valley magnon states [inset in (a) for illustration]. The blue lines in (a) and (b) represent the gapped valley wave mode.

Δ_{pair} is comparable in magnitude to Δ_{HF}, but the former is larger at $\nu = 3$, as shown in Fig. 2(a). We find that the same ($\Delta_{\text{pair}} > \Delta_{\text{HF}}$) is also true at $\nu = 1$ and 2 for spin maximally polarized states. By comparison, Δ_{pair} is half of Δ_{HF} for the $\nu = 1$ quantum Hall ferromagnet in the lowest Landau level with Coulomb interaction [64]. An important difference here with the lowest Landau level is that electron density in the moiré band is spatially nonuniform with modulation within the moiré unit cell, and both the Hartree and Fock self-energies modify the moiré bandwidth. Nevertheless, we find that Δ_{pair} can be tuned to be smaller than Δ_{HF} in TBG by taking both Δ_b and Δ_t to be finite (30 meV), which can be realized when both the top and bottom encapsulating hBN layers are in close alignment to TBG (see Supplemental Material [67] for details). Therefore, we conclude that the lowest charged excitation is determined by either Δ_{HF} or Δ_{pair}, depending on system details.

Valley wave.—In addition to spin magnon states, there are also valley magnon states with a single valley flip

$$|\boldsymbol{Q}\rangle_V = \sum_{\boldsymbol{k}} z_{\boldsymbol{k},\boldsymbol{Q}} c^\dagger_{\boldsymbol{k}+\boldsymbol{Q},+,\downarrow} c_{\boldsymbol{k},-,s} |\nu = 3\rangle, \tag{6}$$

where s can be either $\uparrow$ or $\downarrow$, since both spin components in the $-K$ valley are fully occupied in $|\nu = 3\rangle$. States $|\boldsymbol{Q}\rangle_V$ with $s = \uparrow$ and $\downarrow$ are energetically degenerate for the Hamiltonian H because it actually has an enlarged spin $\mathrm{SU}(2) \times \mathrm{SU}(2)$ symmetry (independent spin rotation within each valley). The corresponding Bethe-Salpeter equation is given by

$$\mathcal{E}_V(\boldsymbol{Q}) z_{\boldsymbol{k},\boldsymbol{Q}} = \sum_{\boldsymbol{k}'} \mathcal{W}^{(\boldsymbol{Q})}_{\boldsymbol{k}\boldsymbol{k}'} z_{\boldsymbol{k}',\boldsymbol{Q}},$$
$$\mathcal{W}^{(\boldsymbol{Q})}_{\boldsymbol{k}\boldsymbol{k}'} = (E_{\boldsymbol{k}+\boldsymbol{Q},+,\downarrow} - E_{\boldsymbol{k},-,s}) \delta_{\boldsymbol{k},\boldsymbol{k}'} - \frac{1}{A} V^{(-+)}_{\boldsymbol{k}'(\boldsymbol{k}+\boldsymbol{Q})(\boldsymbol{k}'+\boldsymbol{Q})\boldsymbol{k}}, \tag{7}$$

which leads to the valley excitation spectrum in Fig. 4. In contrast to the spin excitation spectrum, the lowest valley excitation mode (valley wave) is *gapped*, consistent with the fact that there is no continuous symmetry broken in the valley pseudospin space. The positive-energy valley wave indicates the robustness of $\nu = 3$ QAHF against small variation in the valley space, which implies that the valley polarized state is energetically more favorable than the valley coherent state [53]. The valley wave can again be described by a nonlinear sigma model but with an Ising anisotropy

$$\mathcal{L}_V = -\int d^2\boldsymbol{r} \Big\{ \frac{\hbar n_0}{2} \boldsymbol{\mathcal{A}}[\boldsymbol{\pi}] \cdot \partial_t \boldsymbol{\pi} - u\pi_z^2 + \frac{\rho_z}{2} (\boldsymbol{\nabla}\pi_z)^2 + \frac{\rho_\perp}{2} [(\boldsymbol{\nabla}\pi_x)^2 + (\boldsymbol{\nabla}\pi_y)^2] \Big\}, \tag{8}$$

where the unit vector $\boldsymbol{\pi}$ represents the local valley polarization (π_z for valley Ising order and $\pi_{x,y}$ for valley coherent order), $u > 0$ captures the Ising anisotropy, $\rho_{z,\perp}$ are anisotropic valley stiffness, and other terms are similar to those in Eq. (5). The analytical valley wave dispersion is $\mathcal{E}_{\text{VW}} = \Delta_V + (2\rho_\perp/n_0)\boldsymbol{Q}^2$, where $\Delta_V = 4u/n_0$. Therefore, we can estimate u and $\rho_\perp$ using the numerical valley excitation spectrum in Fig. 4.

Because of the Ising anisotropy, there can be valley domain excitations. We make a domain wall ansatz $(\pi_x, \pi_y, \pi_z) = [\mathrm{sech}(x/\lambda), 0, \tanh(x/\lambda)]$, and its energy cost is minimized by taking the domain wall width λ to be $\sqrt{(\rho_\perp + 2\rho_z)/(6u)}$. The domain wall energy per length is then $J = 4u\lambda$. We note that this domain wall separates regions with opposite Chern numbers and binds one-dimensional chiral electronic states. The valley Ising ordering temperature limited by the proliferation of domain walls can be estimated to be [71,72]

$$k_B T_{\text{DW}} = \frac{2}{\ln(1+\sqrt{2})} J\lambda \approx 2.62 \left(\frac{\lambda}{a_M}\right)^2 \Delta_V, \tag{9}$$

where a_M is the moiré period. Δ_V can be directly extracted from the valley wave spectrum, but λ cannot because $\mathcal{E}_{\text{VW}}$ has no dependence on ρ_z. Since a_M is the lattice scale in our problem, we argue that the domain wall width λ is larger

than a_M, and therefore, we estimate that $k_B T_{\mathrm{DW}} > 2.62\Delta_V$. On the other hand, valley waves are already thermally excited when $k_B T$ exceeds Δ_V. Therefore, we conclude that the valley ordering temperature T_V is mostly limited by valley waves instead of domain walls, and estimate $k_B T_V$ from the valley wave minimum energy. The resulting T_V is shown in Fig. 2(b), which is below the mean-field transition temperature T_{MF}. For a zero-temperature charged excitation gap of 2 meV, we find a corresponding T_V of about 11 K, which compares well with the experimental Curie temperature [8]. Although this good quantitative agreement with experiment might be a coincidence, our work establishes the emergent TBG QAHF to be likely a valley Ising ordered state. Regarding the finite jump in the experimentally measured R_{xy} near the transition temperature [8], we provide a possible theoretical scenario that the interplay between the continuous spin order parameter $\boldsymbol{m}$ and the Ising degree of freedom π_z through higher-order coupling terms (not included in $\mathcal{L}_S$ and $\mathcal{L}_V$) could change the finite-temperature phase transition from second order to first order [73].

Discussion.—In summary, we present a microscopic theory for spin and valley waves of QAHF in TBG and demonstrate that the excitation spectra provide important information about the stability of mean-field state, the transport energy gap, and the valley ordering temperature. We find that TBG QAHF is robust, provided that other effects such as disorder can be neglected. In addition to ferromagnetism, flat moiré bands can host a rich set of broken symmetry states. Our theory can be generalized to study collective excitations of other broken symmetry states in moiré materials.

F. W. thanks A. Young, M. Zaletel, N. Bultinck, S. Chatterjee and I. Martin for discussions. This work was initiated at the Aspen Center for Physics, which is supported by National Science Foundation Grant No. PHY-1607611. We acknowledge support by the Laboratory for Physical Sciences.

Note added.—Recently, three related arXiv preprints [74–76] appeared. In this Letter, we addressed valley ordering temperature limited by valley wave excitations, which has not been studied previously in TBG to our knowledge.

[1] Y. Cao, V. Fatemi, S. Fang, K. Watanabe, T. Taniguchi, E. Kaxiras, and P. Jarillo-Herrero, Nature (London) **556**, 43 (2018).
[2] Y. Cao, V. Fatemi, A. Demir, S. Fang, S. L. Tomarken, J. Y. Luo, J. D. Sanchez-Yamagishi, K. Watanabe, T. Taniguchi, E. Kaxiras, R. C. Ashoori, and P. Jarillo-Herrero, Nature (London) **556**, 80 (2018).
[3] A. Kerelsky, L. J. McGilly, D. M. Kennes, L. Xian, M. Yankowitz, S. Chen, K. Watanabe, T. Taniguchi, J. Hone, C. Dean, A. Rubio, and A. N. Pasupathy, Nature (London) **572**, 95 (2019).
[4] Y. Choi, J. Kemmer, Y. Peng, A. Thomson, H. Arora, R. Polski, Y. Zhang, H. Ren, J. Alicea, G. Refael *et al.*, Nat. Phys. **15**, 1174 (2019).
[5] Y. Cao, D. Chowdhury, D. Rodan-Legrain, O. Rubies-Bigordà, K. Watanabe, T. Taniguchi, T. Senthil, and P. Jarillo-Herrero, arXiv:1901.03710 [Phys. Rev. Lett. (to be published)].
[6] H. Polshyn, M. Yankowitz, S. Chen, Y. Zhang, K. Watanabe, T. Taniguchi, C. R. Dean, and A. F. Young, Nat. Phys. **15**, 1011 (2019).
[7] A. L. Sharpe, E. J. Fox, A. W. Barnard, J. Finney, K. Watanabe, T. Taniguchi, M. A. Kastner, and D. Goldhaber-Gordon, Science **365**, 605 (2019).
[8] M. Serlin, C. Tschirhart, H. Polshyn, Y. Zhang, J. Zhu, K. Watanabe, T. Taniguchi, L. Balents, and A. Young, Science, eaay5533 (2019), https://doi.org/10.1126/science.aay5533.
[9] G. Chen, A. L. Sharpe, E. J. Fox, Y.-H. Zhang, S. Wang, L. Jiang, B. Lyu, H. Li, K. Watanabe, T. Taniguchi *et al.*, arXiv:1905.06535.
[10] M. Yankowitz, S. Chen, H. Polshyn, Y. Zhang, K. Watanabe, T. Taniguchi, D. Graf, A. F. Young, and C. R. Dean, Science **363**, 1059 (2019).
[11] E. Codecido, Q. Wang, R. Koester, S. Che, H. Tian, R. Lv, S. Tran, K. Watanabe, T. Taniguchi, F. Zhang *et al.*, arXiv:1902.05151.
[12] X. Lu, P. Stepanov, W. Yang, M. Xie, M. A. Aamir, I. Das, C. Urgell, K. Watanabe, T. Taniguchi, G. Zhang *et al.*, Nature (London) **574**, 653 (2019).
[13] S. L. Tomarken, Y. Cao, A. Demir, K. Watanabe, T. Taniguchi, P. Jarillo-Herrero, and R. C. Ashoori, Phys. Rev. Lett. **123**, 046601 (2019).
[14] Y. Xie, B. Lian, B. Jäck, X. Liu, C.-L. Chiu, K. Watanabe, T. Taniguchi, B. A. Bernevig, and A. Yazdani, Nature (London) **572**, 101 (2019).
[15] Y. Jiang, X. Lai, K. Watanabe, T. Taniguchi, K. Haule, J. Mao, and E. Y. Andrei, Nature (London) **573**, 91 (2019).
[16] C. Shen, N. Li, S. Wang, Y. Zhao, J. Tang, J. Liu, J. Tian, Y. Chu, K. Watanabe, T. Taniguchi *et al.*, arXiv:1903.06952.
[17] X. Liu, Z. Hao, E. Khalaf, J. Y. Lee, K. Watanabe, T. Taniguchi, A. Vishwanath, and P. Kim, arXiv:1903.08130.
[18] Y. Cao, D. Rodan-Legrain, O. Rubies-Bigordà, J. M. Park, K. Watanabe, T. Taniguchi, and P. Jarillo-Herrero, arXiv:1903.08596.
[19] C. Xu and L. Balents, Phys. Rev. Lett. **121**, 087001 (2018).
[20] H. C. Po, L. Zou, A. Vishwanath, and T. Senthil, Phys. Rev. X **8**, 031089 (2018).
[21] M. Koshino, N. F. Q. Yuan, T. Koretsune, M. Ochi, K. Kuroki, and L. Fu, Phys. Rev. X **8**, 031087 (2018).
[22] J. Kang and O. Vafek, Phys. Rev. X **8**, 031088 (2018).
[23] C.-C. Liu, L.-D. Zhang, W.-Q. Chen, and F. Yang, Phys. Rev. Lett. **121**, 217001 (2018).
[24] J. F. Dodaro, S. A. Kivelson, Y. Schattner, X. Q. Sun, and C. Wang, Phys. Rev. B **98**, 075154 (2018).
[25] H. Isobe, N. F. Q. Yuan, and L. Fu, Phys. Rev. X **8**, 041041 (2018).
[26] Y.-Z. You and A. Vishwanath, npj Quantum Mater. **4**, 16 (2019).

[27] Q.-K. Tang, L. Yang, D. Wang, F.-C. Zhang, and Q.-H. Wang, Phys. Rev. B **99**, 094521 (2019).
[28] L. Rademaker and P. Mellado, Phys. Rev. B **98**, 235158 (2018).
[29] F. Guinea and N. R. Walet, Proc. Natl. Acad. Sci. U.S.A. **115**, 13174 (2018).
[30] J. González and T. Stauber, Phys. Rev. Lett. **122**, 026801 (2019).
[31] Y. Su and S.-Z. Lin, Phys. Rev. B **98**, 195101 (2018).
[32] A. Ramires and J. L. Lado, Phys. Rev. Lett. **121**, 146801 (2018).
[33] G. Tarnopolsky, A. J. Kruchkov, and A. Vishwanath, Phys. Rev. Lett. **122**, 106405 (2019).
[34] J. Ahn, S. Park, and B.-J. Yang, Phys. Rev. X **9**, 021013 (2019).
[35] Z. Song, Z. Wang, W. Shi, G. Li, C. Fang, and B. A. Bernevig, Phys. Rev. Lett. **123**, 036401 (2019).
[36] K. Hejazi, C. Liu, H. Shapourian, X. Chen, and L. Balents, Phys. Rev. B **99**, 035111 (2019).
[37] Y. Sherkunov and J. J. Betouras, Phys. Rev. B **98**, 205151 (2018).
[38] J. Kang and O. Vafek, Phys. Rev. Lett. **122**, 246401 (2019).
[39] K. Seo, V. N. Kotov, and B. Uchoa, Phys. Rev. Lett. **122**, 246402 (2019).
[40] Y.-P. Lin and R. M. Nandkishore, Phys. Rev. B **100**, 085136 (2019).
[41] T. J. Peltonen, R. Ojajärvi, and T. T. Heikkilä, Phys. Rev. B **98**, 220504(R) (2018).
[42] B. Lian, Z. Wang, and B. A. Bernevig, Phys. Rev. Lett. **122**, 257002 (2019).
[43] Y. W. Choi and H. J. Choi, Phys. Rev. B **98**, 241412(R) (2018).
[44] F. Wu, A. H. MacDonald, and I. Martin, Phys. Rev. Lett. **121**, 257001 (2018).
[45] F. Wu, E. Hwang, and S. Das Sarma, Phys. Rev. B **99**, 165112 (2019).
[46] F. Wu, Phys. Rev. B **99**, 195114 (2019).
[47] F. Wu and S. Das Sarma, Phys. Rev. B **99**, 220507(R) (2019).
[48] F. Wu and S. Das Sarma, arXiv:1906.07302.
[49] Y.-H. Zhang, D. Mao, Y. Cao, P. Jarillo-Herrero, and T. Senthil, Phys. Rev. B **99**, 075127 (2019).
[50] B. L. Chittari, G. Chen, Y. Zhang, F. Wang, and J. Jung, Phys. Rev. Lett. **122**, 016401 (2019).
[51] F. Wu, T. Lovorn, E. Tutuc, I. Martin, and A. H. MacDonald, Phys. Rev. Lett. **122**, 086402 (2019).
[52] M. Xie and A. H. MacDonald, arXiv:1812.04213.
[53] N. Bultinck, S. Chatterjee, and M. P. Zaletel, arXiv:1901.08110.
[54] Y.-H. Zhang, D. Mao, and T. Senthil, Phys. Rev. Research **1**, 033126 (2019).
[55] J. Liu, Z. Ma, J. Gao, and X. Dai, Phys. Rev. X **9**, 031021 (2019).
[56] J. Y. Lee, E. Khalaf, S. Liu, X. Liu, Z. Hao, P. Kim, and A. Vishwanath, Nat. Commun. **10**, 5333 (2019).
[57] X.-C. Wu, A. Keselman, C.-M. Jian, K. A. Pawlak, and C. Xu, Phys. Rev. B **100**, 024421 (2019).
[58] T. Hazra, N. Verma, and M. Randeria, Phys. Rev. X **9**, 031049 (2019).
[59] F. Xie, Z. Song, B. Lian, and B. A. Bernevig, arXiv:1906.02213.
[60] A. Julku, T. J. Peltonen, L. Liang, T. T. Heikkilä, and P. Törmä, arXiv:1906.06313 [Phys. Rev. B (to be published)].
[61] X. Hu, T. Hyart, D. I. Pikulin, and E. Rossi, Phys. Rev. Lett. **123**, 237002 (2019).
[62] J. Liu and X. Dai, arXiv:1907.08932.
[63] C.-Z. Chang *et al.*, Science **340**, 167 (2013).
[64] K. Moon, H. Mori, K. Yang, S. M. Girvin, A. H. MacDonald, L. Zheng, D. Yoshioka, and S.-C. Zhang, Phys. Rev. B **51**, 5138 (1995).
[65] K. Yang, S. Das Sarma, and A. H. MacDonald, Phys. Rev. B **74**, 075423 (2006).
[66] R. Bistritzer and A. H. MacDonald, Proc. Natl. Acad. Sci. U.S.A. **108**, 12233 (2011).
[67] See Supplemental Material at http://link.aps.org/supplemental/10.1103/PhysRevLett.124.046403 for details of the TBG moiré Hamiltonian and an analysis of QAHF in TBG that is closely aligned to both the top and bottom encapsulating hBN layers.
[68] B. Hunt, J. D. Sanchez-Yamagishi, A. F. Young, M. Yankowitz, B. J. LeRoy, K. Watanabe, T. Taniguchi, P. Moon, M. Koshino, P. Jarillo-Herrero, and R. C. Ashoori, Science **340**, 1427 (2013).
[69] A. Srivastava and A. Imamoğlu, Phys. Rev. Lett. **115**, 166802 (2015).
[70] S. M. Girvin, *Topological Aspects of Low Dimensional Systems* (Springer, New York, 1999), pp. 53–175.
[71] P. Chaikin and T. C. Lubensky, *Principles of Condensed Matter Physics* (Cambridge University Press, Cambridge, England, 2000).
[72] X. Li, F. Zhang, Q. Niu, and A. H. MacDonald, Phys. Rev. Lett. **113**, 116803 (2014).
[73] Y. Kato, I. Martin, and C. D. Batista, Phys. Rev. Lett. **105**, 266405 (2010).
[74] C. Repellin, Z. Dong, Y.-H. Zhang, and T. Senthil, arXiv:1907.11723.
[75] Y. Alavirad and J. D. Sau, arXiv:1907.13633.
[76] S. Chatterjee, N. Bultinck, and M. P. Zaletel, arXiv:1908.00986.